Nonequispaced curvelet transform for seismic data reconstruction: a sparsity-promoting approach

Gilles Hennenfent[1], *Lloyd Fenelon*[2], *and Felix J. Herrmann*[3]

[1]Formerly at the Seismic Laboratory for Imaging and Modeling, Department of Earth and Ocean Sciences, the University of British Columbia, 6339 Stores Road, Vancouver, V6T 1Z4, BC, Canada. Now at Chevron Energy Technology Company, 6001 Bollinger Canyon, San Ramon, CA 94583, USA. Email: ghennenfent@chevron.com

[2]Formerly at the École Nationale Supérieure de Physique de Strasbourg, Pole API, Boulevard Sébastien Brant, 67400 Illkirch-Graffenstaden, France, visiting the University of British Columbia. Now at British Columbia Cancer Research Centre, 675 West 10th Avenue, Vancouver, V5T 1L3, BC, Canada. Email: lloyd.fenelon@hotmail.fr

[3]Seismic Laboratory for Imaging and Modeling, Department of Earth and Ocean Sciences, the University of British Columbia, 6339 Stores Road, Vancouver, V6T 1Z4, BC, Canada. Email: fherrmann@eos.ubc.ca

SVN repository: https://wave.eos.ubc.ca/SLIM/SLIM.Papers.nfdct/paper.tex (v.51)

ABSTRACT

Seismic data are typically irregularly sampled along spatial axes. This irregular sampling may adversely affect some key steps, e.g., multiple prediction/attenuation or imaging, in the processing workflow. To overcome this problem almost every large dataset is regularized and/or interpolated.

Our contribution is twofold. Firstly, we extend our earlier work on the nonequispaced fast discrete curvelet transform (NFDCT) and introduce a second generation of the transform. This new generation differs from the previous one by the approach taken to compute accurate curvelet coefficients from irregularly sampled data. The first generation relies on accurate Fourier coefficients obtained by an ℓ_2-regularized inversion of the nonequispaced fast Fourier transform, while the second is based on a direct, ℓ_1-regularized inversion of the operator that links curvelet coefficients to irregular data. Also, by construction, the NFDCT second generation is lossless, unlike the NFDCT first generation. This property is particularly attractive for processing irregularly sampled seismic data in the curvelet domain and bringing them back to their irregular recording locations with high fidelity.

Secondly, we combine the NFDCT second generation with the standard fast discrete curvelet transform (FDCT) to form a new curvelet-based method, coined nonequispaced curvelet reconstruction with sparsity-promoting inversion (NCRSI), for the regularization and interpolation of irregularly sampled data. We demonstrate that, for a pure regularization problem, the reconstruction is very accurate. The signal-to-reconstruction error ratio is, in our example, above 40 dB. We also conduct combined interpolation and regularization experiments. The reconstructions for synthetic data are accurate, particularly when the recording locations are optimally jittered. The reconstruction in our real data example shows amplitudes along the main wavefronts smoothly varying with no obvious acquisition imprint; a result very competitive with results from other reconstruction methods overall.

INTRODUCTION

In the past few years, the seismic industry almost entirely switched from 2-D to 3-D data acquisition geometries. The motivation of this transition came from the substantial increase in information and accuracy of 3-D subsurface images. Unfortunately, these improvements came at a price. Realistic 3-D acquisition geometries are typically much coarser and irregular than their 2-D counterparts, which exacerbates processing difficulties.

If the source and receiver coverage above the target area is not dense enough, the recorded data is aliased and the resulting subsurface image may lose spatial resolution or even be corrupted by artifacts. Irregular sampling yields uneven illumination of the subsurface that creates distortions, referred to as acquisition footprint. It also leads to

poor levels of repeatability between time-lapse, or so-called 4-D, surveys. To overcome these problems, virtually every large dataset is regularized and/or interpolated.

The regularization process, also called bin centering, moves traces from their irregular recording locations to locations on a regular grid. The traces may be altered depending on the method used and some traces may be discarded. The interpolation process interleaves recorded traces with synthesized traces so that the spatial sampling increases. Combined, these processes often have a significant impact on pre-stack time migration (Symes, 2007), 3-D surface-related multiple elimination (SRME - Berkhout and Verschuur, 1997; Verschuur and Berkhout, 1997), wave-equation pre-stack depth migration (Claerbout, 1971), and time-lapse where interpolation and regularization homogenize the sampling between all vintages of the 4-D dataset.

There exists a wide variety of wavefield reconstruction techniques. A simple and widely-used method is flex binning. This fast method handles empty bins. However, it discards the actual recording locations and is only a low dip and low frequency approximation to the reconstruction problem. Other more amplitude- and dip-friendly options are filter-based methods (Claerbout, 1992; Spitz, 1991). These methods are typically used to interpolate regularly sampled data to a finer grid. Wavefield-operator-based methods are arguably the best interpolators because they combine the exact positions of existing traces with the physics of wave propagation to create new traces. They are quite a bit more computationally extensive than transform-based methods though. Transform-based methods (Thorson and Claerbout, 1985; Hampson, 1986; Sacchi et al., 1998; Schonewille, 2000; Trad et al., 2003; Zwartjes, 2005; Herrmann and Hennenfent, 2008) do not capitalize on any particular geophysical model and may relate to the physics of wave propagation depending on the transform used—e.g., Fourier modes correspond to eigenfunctions of a wave equation with constant velocity. Most of aforementioned methods can also regularize but it is not the case of the curvelet reconstruction with sparsity-promoting inversion (CRSI - Herrmann and Hennenfent, 2008).

The objective of this paper is twofold: 1) present an improvement upon the nonequispaced fast discrete curvelet transform (NFDCT) first generation (Hennenfent and Herrmann, 2006) that we referred to as the NFDCT second generation; and 2) introduce a new curvelet-based method, coined nonequispaced curvelet reconstruction with sparsity-promoting inversion (NCRSI), for the regularization and interpolation of irregularly sampled data. NCRSI relies on the NFDCT second generation. To keep the discussion as clear and concise as possible, we focus on the 2-D curvelet transform and 2-D reconstruction of seismic data that are regularly sampled along one axis, time, and irregularly sampled along the other, one spatial coordinate. The extension of our work to more axes irregularly sampled is straightforward, as we briefly explain.

Outline

After an overview of the curvelet transform and its properties, we discuss some of the existing discrete implementations and concentrate on one in particular, the fast discrete curvelet transform (FDCT) via wrapping (Candès et al., 2006), for which we review the NFDCT first generation and present our update. Finally, we introduce NCRSI and illustrate it for regularization and interpolation of synthetic and real data.

CURVELET TRANSFORM

The curvelet transform is a generalization, in 2-D and higher dimensions, of the wavelet transform (Mallat, 1999). It was introduced to approximate, in a non-adaptive manner, curved singularities—e.g., wavefronts—with very few curvelet coefficients (Candès and Donoho, 2000, 2004). The most recent discrete implementations of the transform are presented in Candès et al. (2006) and Ying et al. (2005). Similar transform elements to curvelets were introduced earlier in Smith (1998) as approximate eigenfunctions of Fourier integral operators (FIO); FIO's are high-frequency asymptotic solution operators of the wave equation. Other analogous constructions to curvelets include contourlets (Do and Vetterli, 2002), surfacelets (Lu and Do, 2007), and, more recently, shearlets (Guo et al., 2006; Guo and Labate, 2007). In the remainder of this paper we focus on the 2-D curvelet transform, unless otherwise stated.

General description

The curvelet transform is a multiscale, multidirectional, and localized transform. It corresponds to a specific tilling of the f-k domain into scales that are dyadic bands—i.e., bands whose radial width doubles every scale—centered around the DC point. These scales are subsequently broken up into parabolic angular wedges. The term parabolic refers to the relation between the length and width of a wedge, i.e., length $\propto$ width^2. Figure 1 sketches the resulting curvelet tilling of the f-k domain. Because of the parabolic scaling, the number of wedges doubles every other scale and the curvelets, which live in wedges, become more and more anisotropically shaped. Figure 2 shows a few sample curvelets in the t-x domain (Figure 2(a)) and their imprint in the f-k domain (Figure 2(b)).

In the t-x domain, curvelets form a family of coherent waveforms, also referred to as wave packets (Smith, 1998; Córdoba and Fefferman, 1978). Loosely speaking, these waveforms are anisotropic dilations, rotations, and translations of a mother waveform. Hence, curvelets are indexed by $\gamma \stackrel{\text{def}}{=} (j, l, \mathbf{k}) \in \mathcal{M}$ with $\mathcal{M}$ the multi-index set running over the scale parameter j, the orientation parameter l, and the translation parameter $\mathbf{k} \stackrel{\text{def}}{=} (k_1, k_2)$. Mathematically, they are tight frame elements. This means that, much like the Fourier transform, the curvelet transform can analyze

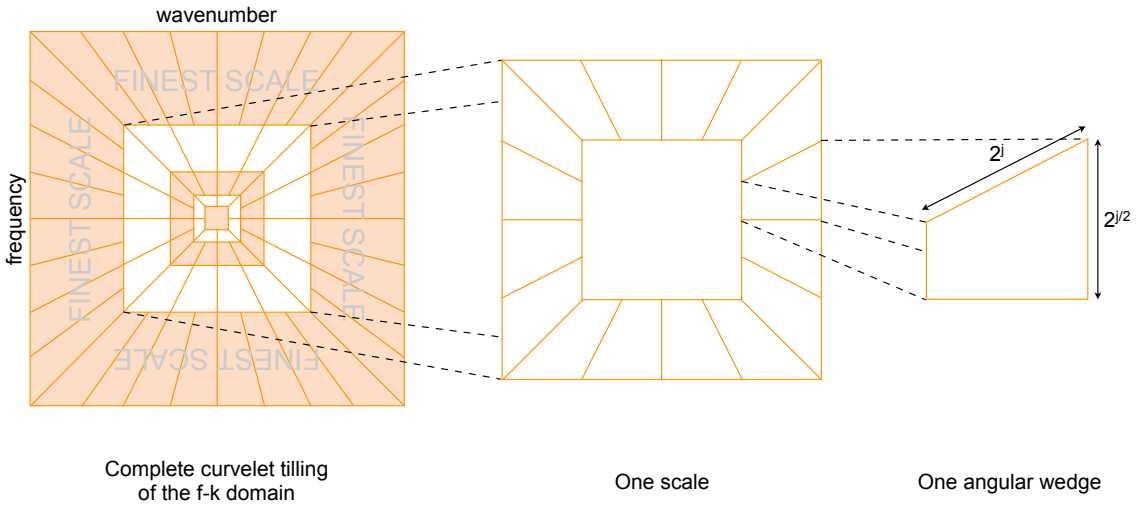

Figure 1: Schematic curvelet tilling of the f-k plane. From left to right: complete DC-centered tilling, j^{th} dyadic scale, and one angular "parabolic" wedge.

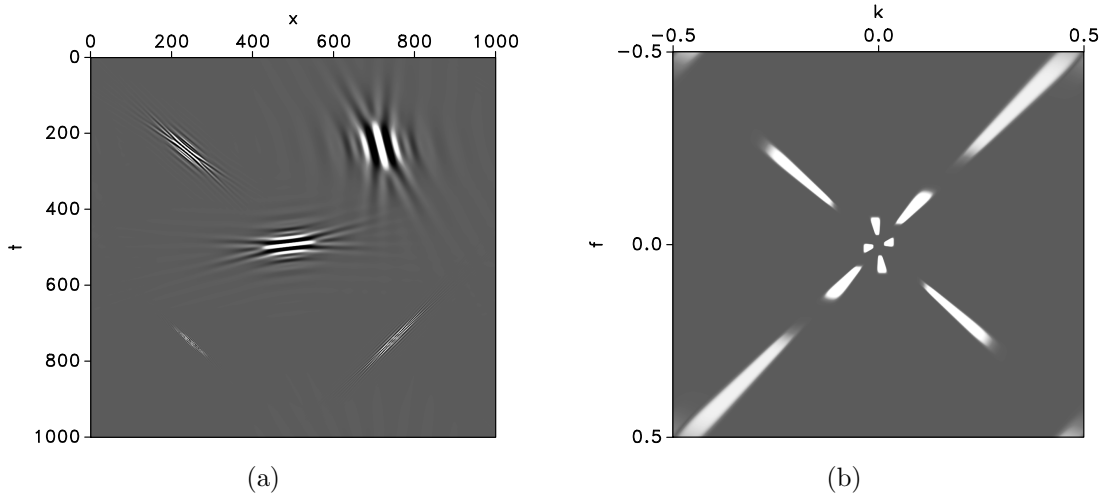

Figure 2: Sample curvelets. (a) Five real curvelets at different scales and angles. (b) Amplitude spectrum of (a).

and synthesize a signal as a superposition of curvelets without loss of information. It is, however, a redundant transformation—i.e., there is more than one way to build a signal as a superposition of curvelets.

Because of the anisotropic scaling law, the directional selectivity, the spatial localization, and the oscillatory nature, curvelets provide an essentially optimal representation of signals that are smooth except along smooth curves (Candès and Donoho, 2004). In particular, curvelets arguably yield the most compressible, non-adaptive representation of seismic data (Hennenfent and Herrmann, 2006; Candès et al., 2006; Douma and de Hoop, 2007). This property is at the core of CRSI and other curvelet-based applications (see e.g., Herrmann et al., 2008, and references therein).

Existing discrete implementations

The first generation of the discrete curvelet transform (Donoho and Duncan, 1999; Starck et al., 2002) is 2-D and relies on the discrete ridgelet transform (Candès, 1998). The resulting operator pair, i.e., synthesis and analysis operators, is faithful to the properties of the continuous transform. It is, however, quite expansive, by a factor of about 16.

More recently, Candès et al. (2006) proposed two new 2-D discrete implementations. One is based on unequally-spaced fast Fourier transforms (FDCT via USFFT), the other on wrapping specially selected Fourier samples (FDCT via wrapping). We focus on the latter implementation for two reasons: 1) it has a 3-D extension (Ying et al., 2005); and 2) it forms a tight frame, unlike FDCT via USFFT.

The FDCT via wrapping is expansive by a factor of about 8 in 2-D. The architecture of its analysis operator is as follows: 1) apply the analysis 2-D fast Fourier transform (FFT); 2) form the angular wedges; 3) wrap each wedge around the origin; and 4) apply the synthesis 2-D FFT to each wedge. The synthesis/adjoint operator—also the inverse owing to the tight-frame property—is computed by reversing these operations. For the purpose of this paper, however, it suffices to define it as

$$\mathbf{A} \stackrel{\text{def}}{=} \mathbf{FT}, \tag{1}$$

where $\mathbf{F}$ is the synthesis 2-D FFT and $\mathbf{T}$ the curvelet tilling operator that maps curvelet coefficients to the f-k domain. Figure 3 sketches this decomposition.

Extension of the FDCT via wrapping to 1-D nonequispaced traces

The FDCT via wrapping cannot be readily used with nonequispaced data because of the 2-D FFT involved in the transform (operator $\mathbf{F}$ in Equation 1). The 2-D FFT assumes a regular sampling along each axes, effectively discarding the actual recording locations of the input traces. The wavefield is deformed or even broken, which

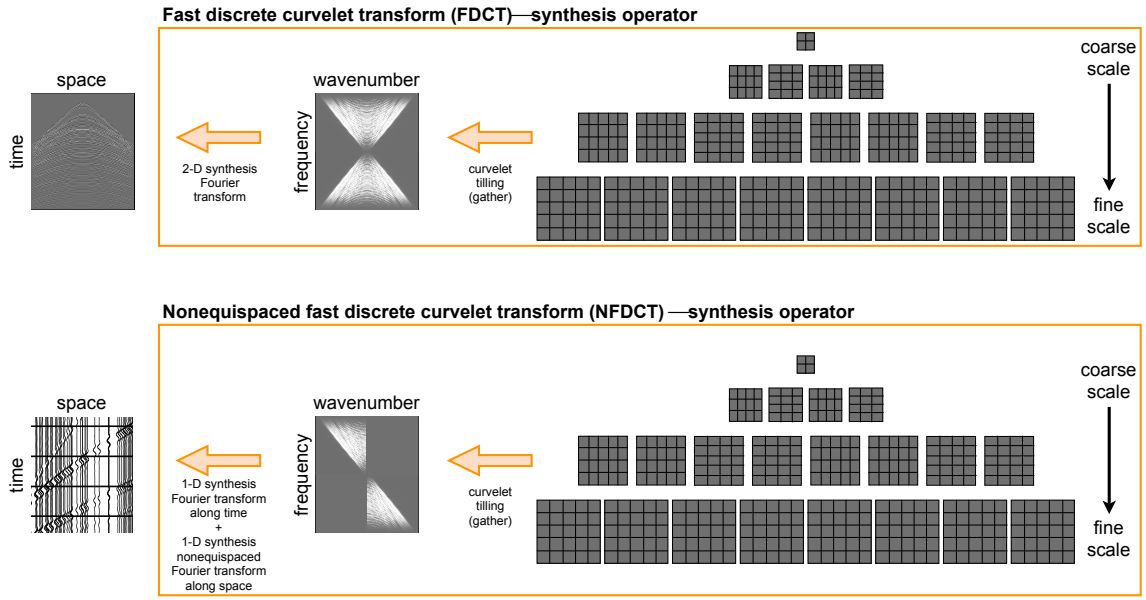

Figure 3: Schematic decomposition of the synthesis FDCT and NFDCT operators. The two operators only differ by the way they internally bring f-k data to the t-x domain.

reduces the effectiveness of the curvelet approximation (Hennenfent and Herrmann, 2006) and, hence, of curvelet-based applications relying on the effectiveness of this approximation.

Hennenfent and Herrmann (2006) note that the synthesis 2-D FFT operator is the Kronecker product, denoted by the symbol $\otimes$, of the synthesis 1-D FFT operator along the temporal axis, $\mathbf{F}_t$, and the synthesis 1-D FFT operator along the spatial axis, $\mathbf{F}_x$, i.e.,

$$\mathbf{F} = \mathbf{F}_x \otimes \mathbf{F}_t. \tag{2}$$

In this decomposition these authors substitute $\mathbf{F}_x$ for the synthesis 1-D nonequispaced fast Fourier transform (NFFT - Potts et al., 2001; Kunis, 2006) along the spatial axis, $\mathbf{N}_x$, and form a new operator

$$\mathbf{B} \stackrel{\text{def}}{=} (\mathbf{N}_x \otimes \mathbf{F}_t)\,\mathbf{T} \tag{3}$$

that links curvelet coefficients to nonequispaced traces (Figure 3). The newly-formed discrete curvelets are sampled like seismic data, as illustrated in Figure 4. The grayscale image represents a regularly sampled curvelet, the overlaid wiggle plot a "seismic" curvelet for an arbitrary spatial sampling.

Because the FDCT via wrapping is a tight frame a roundtrip from the t-x domain is lossless, i.e.,

$$\mathbf{A}\mathbf{A}^H = \mathbf{I} \tag{4}$$

where the symbol ^{H} denotes the conjugate transpose, and the operator $\mathbf{I}$ is the identity matrix. The same property does not hold for $\mathbf{B}$ due to $\mathbf{N}_x$. Concentrating on

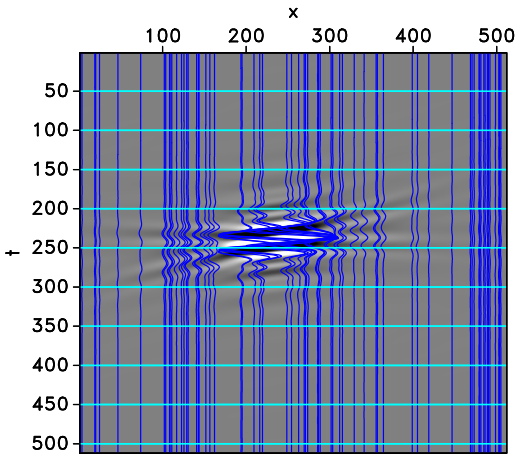

Figure 4: Seismic curvelet. The grayscale image represents a regularly sampled curvelet, the overlaid wiggle plot a "seismic" curvelet for an arbitrary spatial sampling.

the overdetermined case—i.e., more irregular input locations than desired Fourier coefficients—Hennenfent and Herrmann (2006) partially solve this problem by defining another operator, $\mathbf{B'}$, as follows

$$\mathbf{B'} \stackrel{\text{def}}{=} \mathbf{T}^H \left(\mathbf{N}_x^\dagger \otimes \mathbf{F}_t^H \right) \tag{5}$$

to go from the t-x domain to the curvelet domain. The symbol † denotes the weighted least-squares pseudoinverse. In this approach the accuracy of the resulting curvelet coefficients depends upon the accuracy of the Fourier coefficients obtained by the regularized inversion of the NFFT operator. Moreover, the roundtrip may be lossy due to the inversion of an overdetermined linear system.

In this paper, we concentrate on the underdetermined case and define the analysis NFDCT operator, $B^\ddagger$, as

$$B^\ddagger : \mathbf{y} \mapsto \tilde{\mathbf{x}} = \arg\min_{\mathbf{x}} \|\mathbf{x}\|_1 \quad \text{s.t.} \quad \mathbf{y} = \mathbf{B}\mathbf{x}. \tag{6}$$

In words, $B^\ddagger$ nonlinearly maps the recorded data, $\mathbf{y}$, to the curvelet coefficient vector, $\tilde{\mathbf{x}}$, solution of the basis pursuit problem (Chen et al., 1998). By construction the operator pair $\left(B^\ddagger, \mathbf{B}\right)$ is lossless—i.e., the curvelet coefficients obtained in Equation 6 explain exactly the data at irregular locations. We call this pair the NFDCT second generation.

Extension of the NFDCT second generation to higher spatial dimensions

Extending the NFDCT second generation to two or more spatial axes irregularly sampled is straightforward. The synthesis operator is defined as follows

$$\mathbf{C} \stackrel{\text{def}}{=} (\mathbf{N_x} \otimes \mathbf{F}_t)\,\mathbf{T} \tag{7}$$

where $\mathbf{N_x}$ is the synthesis N-D NFFT along N spatial axes. The analysis operator $C^\ddagger$ is obtained by substituting $\mathbf{B}$ for $\mathbf{C}$ in Equation 6.

APPLICATION TO SEISMIC DATA RECONSTRUCTION

In this section, we combine the NFDCT second generation with the standard FDCT to form NCRSI. We illustrate this new regularization and interpolation method on synthetic and real data. One regularization example is followed by several interpolation examples.

Nonequispaced curvelet reconstruction with sparsity-promoting inversion

NCRSI relies on $\tilde{\mathbf{x}}$ in Equation 6 being equal, or at least close, to the curvelet coefficients for the underlying continuous wavefield irregularly sampled in $\mathbf{y}$. In this case, the reconstructed—i.e., interpolated and/or regularized—wavefield, $\tilde{\mathbf{f}}$, is obtained as follows

$$\tilde{\mathbf{f}} = \mathbf{A}B^\ddagger\mathbf{y}. \tag{8}$$

This expression defines NCRSI. As a reminder, $\mathbf{A}$ is the standard synthesis FDCT operator, and $B^\ddagger$ the analysis NFDCT second generation operator. In words, Equation 8 means that the reconstructed wavefield is obtained by applying the standard synthesis operator of the curvelet transform on the smallest ℓ_1-norm curvelet vector that explains the acquired data at their exact recording locations.

Regularization

A synthetic seismic shot (Figure 5) is generated with a finite-difference code for a subsurface velocity model with two-dimensional inhomogeneities. The 250 traces of this reference shot are at the center of 15-meter, contiguous bins and the temporal sampling is 4 ms. These traces are subsequently used to generate 250 new traces that are at random locations within each bin. The nominal spatial sampling remains 15 m.

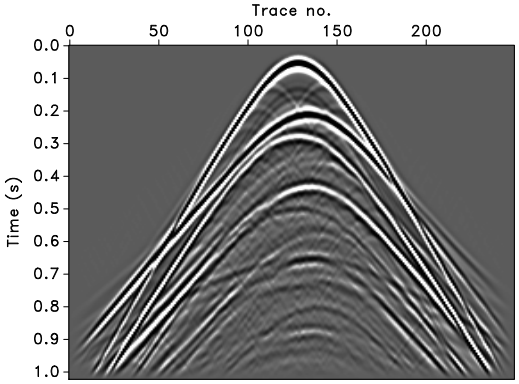

Figure 5: Synthetic seismic shot. This shot is used to demonstrate the effectiveness of the NFDCT second generation in the context of seismic data regularization and/or interpolation on synthetic data.

Figure 6(a) shows the resulting 15-meter binned—using nearest-neighbor interpolation—dataset. Figure 6(c) shows in more details the late times, high trace numbers. The grayscale image in the background is the reference shot, the wiggly traces are the binned data. For further comparison, the difference plot between the reference and regularized shots is shown in Figure 6(e). Because the actual recording locations are discarded, the continuity along wavefronts is broken, yielding a measured signal-to-noise ratio (SNR) of 10.25 dB. The SNR is defined as $20 \cdot \log_{10}\left(\|\mathbf{f}\|_2/\|\mathbf{f}-\tilde{\mathbf{f}}\|_2\right)$, where $\mathbf{f}$ represents the reference shot and $\tilde{\mathbf{f}}$ the regularized shot. The higher the SNR, the more faithful the regularization.

The 15-meter NCRSI result is presented in Figures 6(b) and 6(d). The wavefronts are remarkably continuous. There is virtually no difference between the regularized and reference shots, as corroborated by the difference plot shown in Figure 6(f) and the very high SNR of 42.42 dB.

Interpolation

We first discuss two different interpolation-and-regularization examples on synthetic data. A field data illustration follows.

Synthetic data examples

The reference shot of the regularization example (Figure 5) is used to generate 125 new traces at random locations in every other 15-meter bin. In other words, there is a trace every 30 m $\pm$ 7.5 m so that every other bin is empty. The minimum distance between two consecutive receivers is 15 m, the maximum distance is 45 m. Figure 7(a) shows the resulting 15-meter binned—using nearest-neighbor interpolation—dataset.

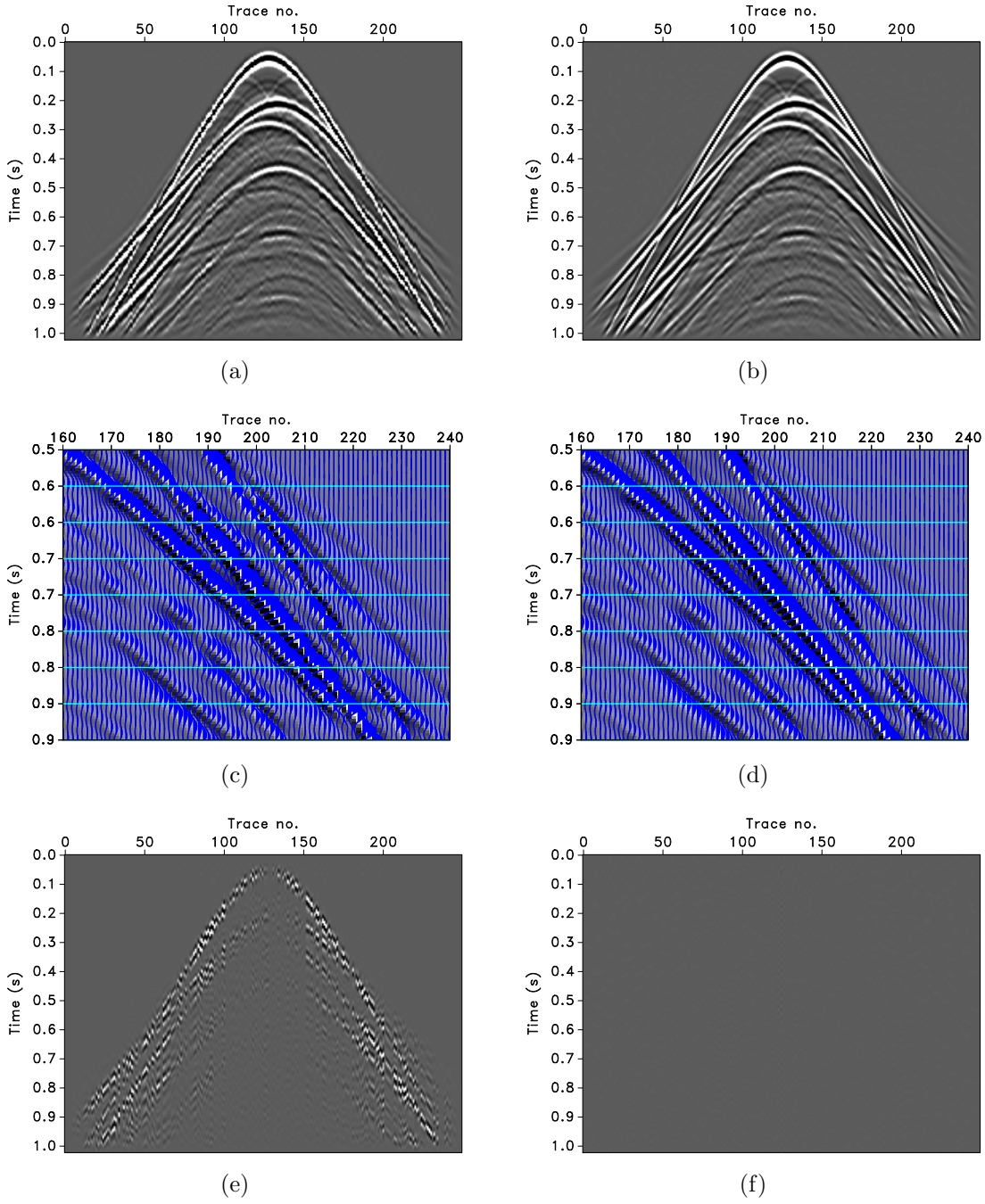

Figure 6: Regularization of synthetic data. (a) Simulated, irregular data 15-meter binned using nearest-neighbor interpolation (nominal spatial sampling: 15 meters), (b) 15-meter NCRSI result. (c) and (d) zooms on late times, high trace numbers. The grayscale image in the background is the reference shot, the wiggly traces are the binned data of (a) and (b), respectively. (e) and (f) are difference plots at the same scale as (a) and (b).

Figure 7(c) is a zoom in late times, high trace numbers. The grayscale image in the background is the reference shot, the wiggly traces are the binned data. Finally, Figure 7(e) is the difference plot between Figures 7(a) and 5. In the even bins, the error is due to missing data whereas, in the odd bins, the error comes from moving traces from the irregular recording locations to the center of the bin without changing them. The measured SNR is 2.6 dB.

For a nominal spatial sampling of 30 m, the data is spatially aliased beyond 25 Hz. Moreover, the irregular recording locations create spectral leakage. The combined interpolation-regularization to a 15-meter regular grid aims at correcting for these two problems and at recovering the wavefield in its full band—i.e., in the frequency range 0 Hz to 50 Hz. Figures 7(b) and 7(d) show the 15-meter NCRSI result. The difference plot is shown in Figure 7(f) and the corresponding SNR is 15.60 dB. Overall, the reconstruction is accurate, although some events are dimmed at early times, in the near offsets.

For interest, we also conduct a combined interpolation-regularization of optimally-jittered data (Hennenfent and Herrmann, 2008). In this case, the nominal spatial sampling is also 30 m. However, the traces are located every 30 m $\pm$ 15 m—i.e., more randomness in the spatial sampling than in our previous example. Two consecutive receivers can be infinitely close but cannot be more than 60 m apart. Figure 8(a) shows the resulting 15-meter binned—using nearest-neighbor interpolation—dataset. Figure 8(c) is a zoom in late times, high trace numbers. The grayscale image in the background is the reference shot, the wiggly traces are the binned data. Finally, Figure 8(e) is the difference plot between Figures 8(a) and 5. The measured SNR is 2.53 dB.

Figures 8(b) and 8(d) show the 15-meter NCRSI result. The difference plot is shown in Figure 8(f) and the corresponding SNR is 16.64 dB. Despite a lower initial SNR, the optimally-jittered data are better interpolated and regularized. The improvement, superior to 1 dB compared to the previous example, is typical of what one can expect for this nominal spatial sampling and data. For more details on jittered sampling of seismic data, we refer to Hennenfent and Herrmann (2008) and Tang et al. (2009).

Real data example

Hindriks and Duijndam (2000), followed by Zwartjes (2005), used a 3-D vertical seismic profile (VSP) dataset to show Fourier reconstruction results of data irregularly sampled along two spatial coordinates. We use the same dataset to illustrate NCRSI. A 2-D subset of the acquired data is shown in Figure 9(a). The nominal spatial sampling is approximately 32 m and the temporal sampling is 8 ms. The reconstruction is performed for the first two seconds in the frequency range 0 Hz to 60 Hz. No minimum velocity is enforced, i.e., the spatial bandwidth is determined by the 20-meter output grid. Because the sampling density is quite variable in the acquired data, we

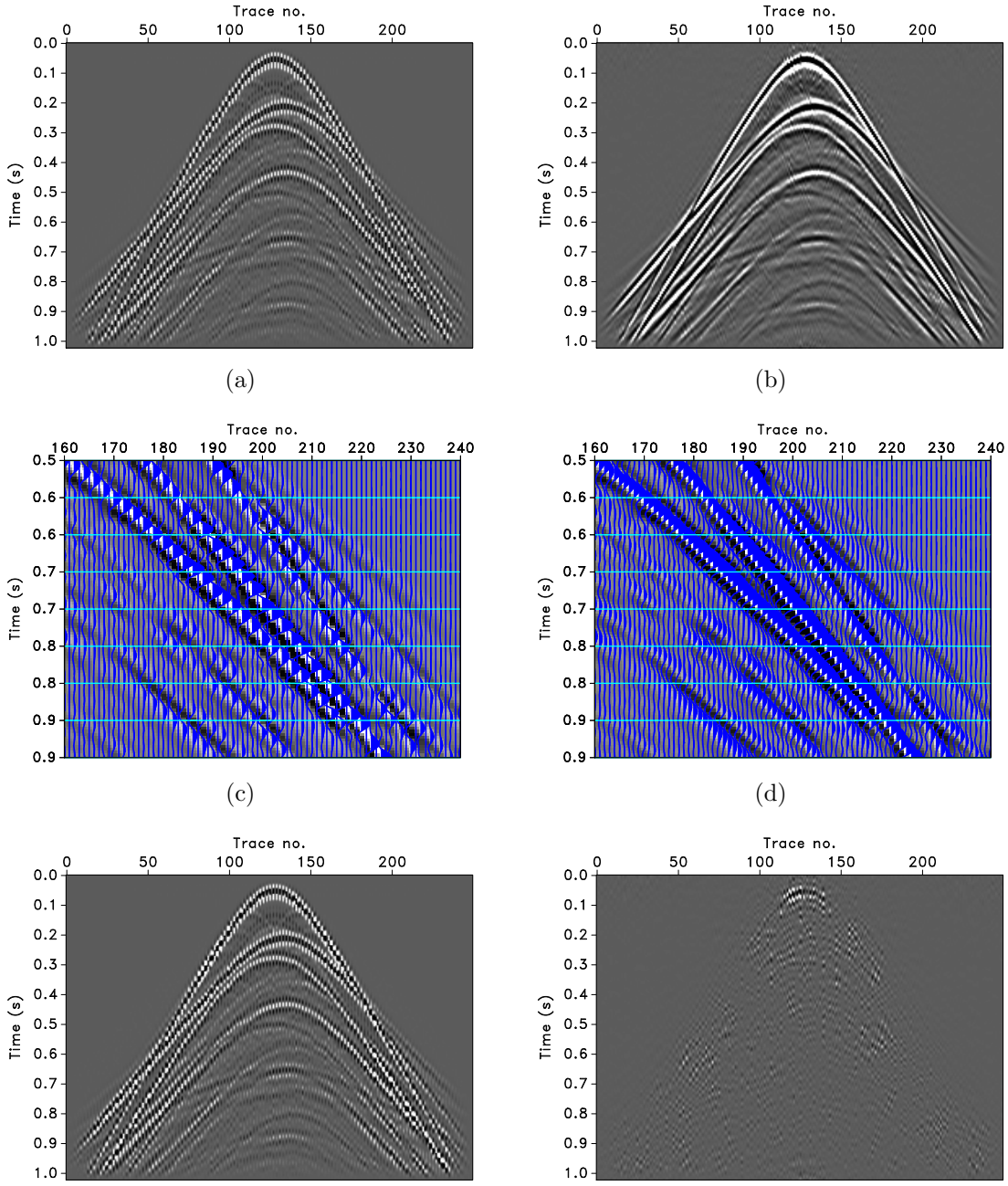

Figure 7: Interpolation and regularization of synthetic data. (a) Simulated, irregular data 15-meter binned using nearest-neighbor interpolation (nominal spatial sampling: 30 m), (b) 15-meter NCRSI result. (c) and (d) zooms on late times, high trace numbers. The grayscale image in the background is the reference shot, the wiggly traces are the binned data of (a) and (b), respectively. (e) and (f) are difference plots at the same scale as (a) and (b).

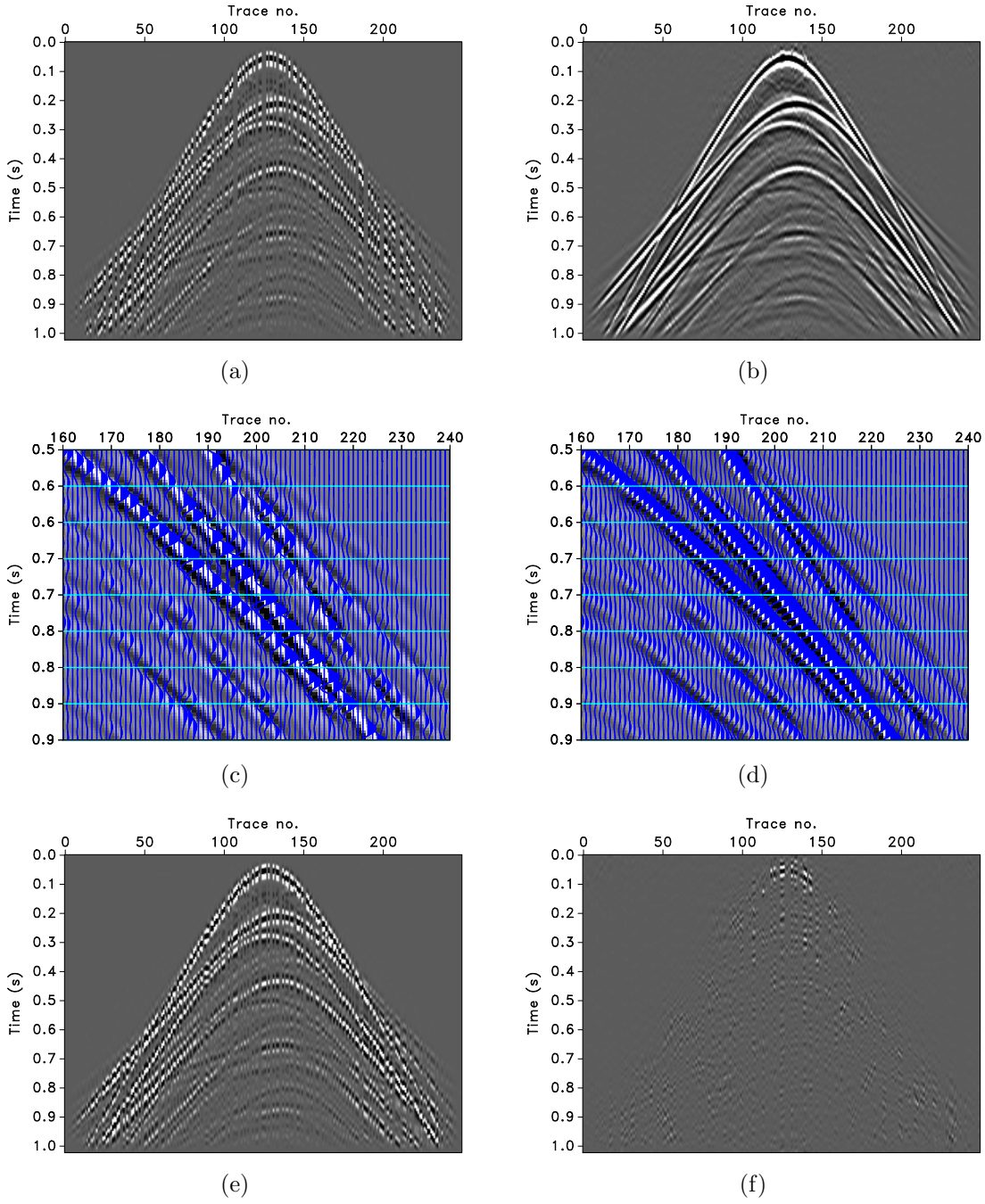

Figure 8: Interpolation and regularization of synthetic, optimally-jittered data. (a) Simulated, irregular data 15-meter binned using nearest-neighbor interpolation (nominal spatial sampling: 30 m), (b) 15-meter NCRSI result. (c) and (d) zooms on late times, high trace numbers. The grayscale image in the background is the reference shot, the wiggly traces are the binned data of (a) and (b), respectively. (e) and (f) are difference plots at the same scale as (a) and (b).

use a left, or so-called data, preconditioner in the definition of $B^\ddagger$ in Equation 6, i.e.,

$$B^\ddagger : \mathbf{y} \mapsto \tilde{\mathbf{x}} = \arg\min_{\mathbf{x}} \|\mathbf{x}\|_1 \quad \text{s.t.} \quad \mathbf{W}\mathbf{y} = \mathbf{W}\mathbf{B}\mathbf{x}. \tag{9}$$

In this formulation, $\mathbf{W}$ is a diagonal weighting matrix. The weights are defined as the average distance to the nearest neighbors (Feichtinger and Grochenig, 1994; Schonewille, 2000; Snieder, 1993) so that it becomes more important to fit accurately an isolated trace than a trace in a dense neighborhood. Figure 9(b) shows the reconstruction using NCRSI. The amplitudes along the main wavefronts are smoothly varying with no obvious acquisition imprint.

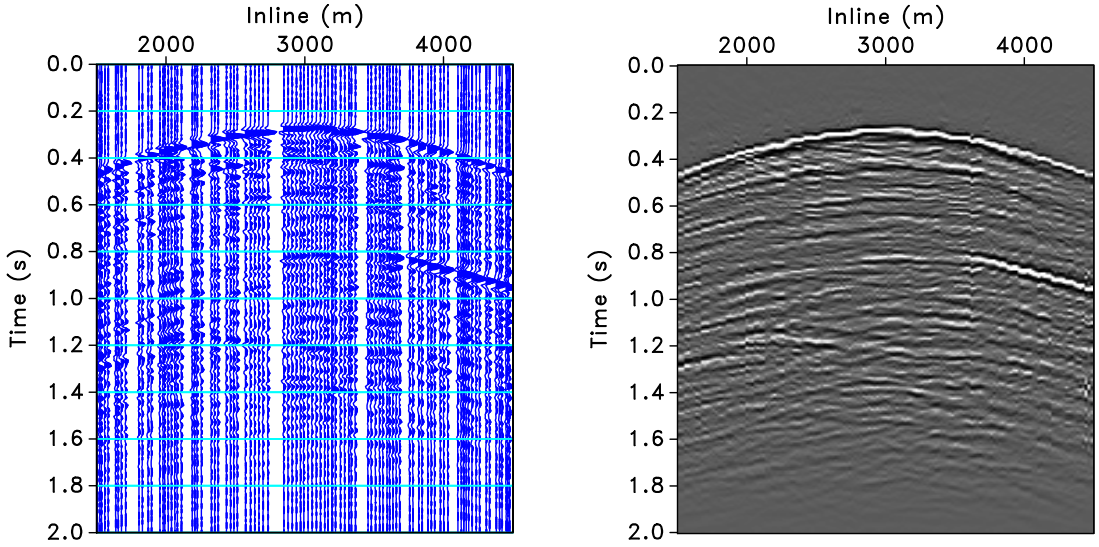

Figure 9: Interpolation and regularization of real data. (a) Acquired data (nominal spatial sampling: approx. 32 m) and (b) 20-meter NCRSI result.

CONCLUSIONS

We introduced the second generation of the nonequispaced fast discrete curvelet transform (NFDCT). The analysis operator of this transform produces accurate curvelet coefficients for irregularly sampled data via a direct, ℓ_1-regularized inversion of the operator that links curvelet coefficients to irregular data. By construction these coefficients explain exactly the data at irregular locations, i.e., the NFDCT second generation is lossless. This property is particularly attractive for processing irregular seismic data in the curvelet domain and bringing them back to irregular locations with high fidelity.

We also proposed a new curvelet-based regularization and interpolation method, coined nonequispaced curvelet reconstruction with sparsity-promoting inversion (NCRSI), that combines the NFDCT second generation with the standard FDCT. We showed

that NCRSI regularizes non-aliased, irregularly sampled data with virtually no error. We also illustrated that the same method produces good interpolated data from aliased and/or irregular input, particularly when the recording locations are optimally jittered.

ACKNOWLEDGMENTS

G.H. thanks Chevron Energy Technology Company for permission to publish this work. This publication was prepared using CurveLab (`curvelet.org`), a toolbox implementing the Fast Discrete Curvelet Transform, NFFT (`www-user.tu-chemnitz.de/~potts/nfft/`), a toolbox implementing the nonequispaced discrete Fourier transform, Madagascar (`rsf.sf.net`), a package for reproducible computational experiments, SPGℓ_1 (`cs.ubc.ca/labs/scl/spgl1`), and Sparco (`cs.ubc.ca/labs/scl/sparco`), a suite of linear operators and problems for testing algorithms for sparse signal reconstruction. This research was in part financially supported by NSERC Discovery Grant 22R81254 and by CRD Grant DNOISE 334810-05 of F.J.H., and was carried out as part of the SINBAD project with support from the following organizations: BG Group, BP, Chevron, Petrobras, and WesternGeco.

REFERENCES

Berkhout, A. J., and D. J. Verschuur, 1997, Estimation of multiple scattering by iterative inversion, part I: Theoretical considerations: Geophysics, **62**, no. 5, 1586–1595.

Candès, E. J., 1998, Ridgelets: theory and applications: PhD thesis, Stanford University, Stanford, CA.

Candès, E. J., L. Demanet, D. L. Donoho, and L. Ying, 2006, Fast discrete curvelet transforms: Multiscale Modeling and Simulation, **5**, no. 3, 861–899.

Candès, E. J., and D. L. Donoho, 2000, Curvelets: a surprisingly effective nonadaptive representation of objects with edges, *in* Curve and surface fitting: Vanderbilt University Press, 105–120.

———, 2004, New tight frames of curvelets and optimal representations of objects with piecewise-C^2 singularities: Communications on Pure and Applied Mathematics, **57**, no. 2, 219–266.

Chen, S. S., D. L. Donoho, and M. A. Saunders, 1998, Atomic decomposition by basis pursuit: SIAM Journal on Scientific Computing, **20**, 33–61.

Claerbout, J. F., 1971, Toward a unified theory of reflector mapping: Geophysics, **36**, no. 3, 467–481.

———, 1992, Earth soundings analysis: processing versus inversion: Blackwell Scientific Publications.

Córdoba, A., and C. Fefferman, 1978, Wave packets and Fourier integral operators: Communications in Partial Differential Equations, **3**, no. 11, 979–1005.

Do, M. N., and M. Vetterli, 2002, Contourlets: a new directional multiresolution

image representation: Proceedings. 2002 International Conference on Image Processing., **1**.

Donoho, D. L., and M. R. Duncan, 1999, Digital curvelet transform: strategy, implementation, and experiments: Technical report, Stanford Statistics Department.

Douma, H., and M. V. de Hoop, 2007, Leading-order seismic imaging using curvelets: Geophysics, **72**, no. 6, S231–S248.

Feichtinger, H. G., and K. Grochenig, 1994, Theory and practice of irregular sampling, *in* Wavelets: mathematics and applications: CRC Press, Studies in Advanced Mathematics, 8, 305–363.

Guo, K., G. Kutyniok, and D. Labate, 2006, Sparse multidimensional representations using anisotropic dilation and shear operators: Wavelets und Splines (Athens, GA, 2005), G. Chen und MJ Lai, eds., Nashboro Press, Nashville, TN, 189–201.

Guo, K., and D. Labate, 2007, Optimally sparse multidimensional representation using shearlets: Journal of Mathematical Analysis, **39**, no. 1, 298–318.

Hampson, D., 1986, Inverse velocity stacking for multiple elimination: Journal of the Canadian Society of Exploration Geophysicists, **22**, no. 1, 44–45.

Hennenfent, G., and F. J. Herrmann, 2006, Seismic denoising with non-uniformly sampled curvelets: Computing in Science and Engineering, **8**, no. 3.

———, 2008, Simply denoise: wavefield reconstruction via jittered undersampling: Geophysics, **73**, no. 3.

Herrmann, F. J., and G. Hennenfent, 2008, Non-parametric seismic data recovery with curvelet frames: Geophysical Journal International, **173**, 233–248.

Herrmann, F. J., D. Wang, G. Hennenfent, and P. P. Moghaddam, 2008, Curvelet-based seismic data processing: a multiscale and nonlinear approach: Geophysics, **73**, no. 1, A1–A5.

Hindriks, K., and A. J. W. Duijndam, 2000, Reconstruction of 3-D seismic signals irregularly sampled along two spatial coordinates: Geophysics, **65**, no. 1, 253–263.

Kunis, S., 2006, Nonequispaced FFT: generalisation and inversion: PhD thesis, Lübeck university.

Lu, Y. M., and M. N. Do, 2007, Multidimensional directional filter banks and surfacelets: IEEE Transactions on Image Processing, **16**, no. 4, 918–931.

Mallat, S., 1999, A wavelet tour of signal processing, second edition: Academic Press.

Potts, D., G. Steidl, and M. Tasche, 2001, Fast Fourier transforms for nonequispaced data: a tutorial, *in* Modern sampling theory: mathematics and applications: Birkhauser, 12, 249–274.

Sacchi, M. D., T. J. Ulrych, and C. J. Walker, 1998, Interpolation and extrapolation using a high-resolution discrete Fourier transform: IEEE Transactions on Signal Processing, **46**, no. 1, 31–38.

Schonewille, M. A., 2000, Fourier reconstruction of irregularly sampled seismic data: PhD thesis, Delft University of Technology, Delft, The Netherlands.

Smith, H., 1998, A hardy space for Fourier integral operators: Journal of Geometric Analysis, **8**, no. 4, 629–653.

Snieder, R., 1993, Global inversions using normal mode and long-period surface waves: Chapman and Hall.

Spitz, S., 1991, Seismic trace interpolation in the FX domain: Geophysics, **56**, no. 6,

785–794.

Starck, J.-L., E. J. Candès, and D. L. Donoho, 2002, The curvelet transform for image denoising: IEEE Transactions on Image Processing, **11**, no. 6, 670–684.

Symes, W. W., 2007, Reverse time migration with optimal checkpointing: Geophysics, **72**, no. 5, SM213–SM221.

Tang, G., R. Shahidi, J. Ma, and F. J. Herrmann, 2009, Design of two-dimensional randomized sampling schemes for curvelet-based sparsity-promoting seismic data recovery: Technical Report TR-2009-03, Earth and Ocean Sciences Department, The University of British Columbia.

Thorson, J. R., and J. F. Claerbout, 1985, Velocity-stack and slant-stack stochastic inversion: Geophysics, **50**, no. 12, 2727–2741.

Trad, D., T. J. Ulrych, and M. D. Sacchi, 2003, Latest views of the sparse Radon transform: Geophysics, **68**, no. 1, 386–399.

Verschuur, D. J., and A. J. Berkhout, 1997, Estimation of multiple scattering by iterative inversion, part II: Practical aspects and examples: Geophysics, **62**, no. 5, 1596–1611.

Ying, L., L. Demanet, and E. J. Candès, 2005, 3-D discrete curvelet transform: Proceedings SPIE wavelets XI, San Diego, **5914**, 344–354.

Zwartjes, P. M., 2005, Fourier reconstruction with sparse inversion: PhD thesis, Delft University of Technology, Delft, The Netherlands.